Crystallization of water in a dynamic diamond-anvil cell: Evidence for ice VII-like local order in supercompressed water

Geun Woo Lee, William J. Evans, and Choong-Shik Yoo
Lawrence Livermore National Laboratory, Livermore, California 94550, USA
(Received 1 June 2006; revised manuscript received 26 July 2006; published 30 October 2006)

We report the observation of ice VII, directly crystallized from metastably supercompressed liquid water at pressure of up to 1.8 GPa, well within the stability field of ice VI. This result is achieved by making time-resolved measurements of pressure-induced crystallization using a unique instrument, a dynamic diamond anvil cell (dDAC), which permits the measurement of pressure/time-dependent phase transformation pathways. We are able to evaluate the interfacial free energy, and find that the value for supercompressed water (SW)/ice VII is smaller than that of SW/ice VI, indicating that the local order of the SW is more similar to ice VII than ice VI. This result is consistent with recent studies, which suggest that the local order of high density water is bcc-like, as in ice VII.

DOI: 10.1103/PhysRevB.74.134112 PACS number(s): 64.70.Dv, 07.35.+k, 61.25.Em, 62.50.+p

INTRODUCTION

H_2O is one of the most fundamental constituents of life and nature, exhibiting profound polymorphism at moderate pressures and temperatures. H_2O has various polymorphs with ordered and disordered forms, exhibiting a range of interesting and unusual physical properties.[1] For example, the discovery of two forms in amorphous ice,[2] low and high density amorphous (LDA and HDA) at low temperatures, is a manifestation of different local structures in amorphous ice and suggests the possibility of a phase transition between these two disordered forms. A recent structural study[3] has clearly demonstrated evidence for the first-order nature of the LDA-HDA phase transition. Analogously, different density forms of liquid water have been suggested experimentally,[4,5] although the structural change occurs continuously.

Local structures of liquid and amorphous solid phases of H_2O are fundamental to understanding its order-disorder phase transition and anomalous phase dynamics, since the similarity in local order between two different phases can favor the selection of a specific phase.[6–8] Previous structural studies have found similar local ordering in LDA and hexagonal ice Ih, and between HDA and liquid water at ambient pressure, based on the observation of overall similarities in the spatial density distribution and partial radial distribution.[9] Using neutron diffraction techniques and Monte Carlo refinement analysis, Klotz *et al.*.[10] concluded that HDA at 0.7 GPa and liquid water at 0 GPa resembled liquid water at 0.4 GPa and HDA at somewhat negative pressures, respectively. Their conclusion suggested that the local structure of HDA is bcc-like, containing broken hydrogen bonds between the first and second nearest neighbor shells, which was also found in ice VII.[10] Interestingly, the metastable ice VII-like (VII′) structure formed from HDA at 4 GPa and 77 K in the pressure-temperature stability regime of ice VIII,[11] which may be interpreted to underscore the analogy of local order between the two phases. Similarly, bcc-like ordering has also been proposed for high density water (HDW) in recent simulation studies.[12–14] However, no experiment has found such local ordering in HDW at high pressures and room temperature. Nor is it apparent whether the local order of HDW is more similar to ice VI or ice VII or ice VIII, which are very different.

To obtain such HDW, liquid water should be compressed far from its equilibrium melting pressure without crystallization, which has not been possible because liquid water readily transforms to ice VI at room temperature as the pressure is increased above melting pressure 0.9 GPa. Thus, it is difficult to form high density metastable water by supercompression of water across the melt line. However, at an elevated rate of compression the kinetic time for nucleation may increase and the metastable liquid may persist for longer without crystallization, as schematically illustrated in the pressure (or, temperature)-time-transformation diagram in Fig. 1. Furthermore, if sufficiently fast, the metastable liquid may entirely pass out of the pressure-temperature stability region of a particular phase and transform to another stable (or even metastable) phase. Experimental examples of this phenomenon include the formation of metastable and stable phase, in supercooled liquid alloys at the ambient pressure,[7,8] and supercompressed liquid water[15] and Ta under shock compression.[16] In this work, we present experimental evidence for supercompressed metastable water (SW) at

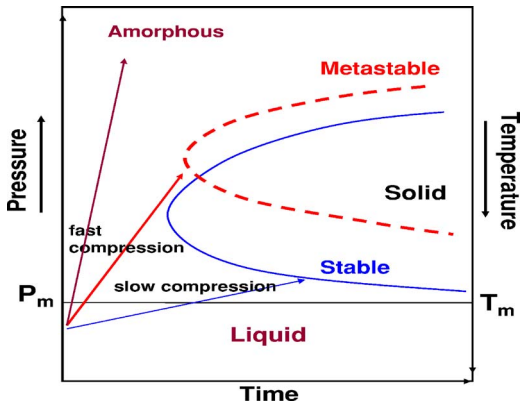

FIG. 1. (Color online) Schematic of the pressure (or temperature)-time transformation diagram, illustrating the transition dynamics, which can give rise to metastable and/or amorphous phases depending on the de/compression (or, cooling) rate.

1.8 GPa, well beyond the melt line at "relatively" slow compression rates (~0.16 GPa/s). Surprisingly, this metastable dense water directly transforms to ice VII within the stability field of ice VI, remarkably similar to the pressure-induced transition from HDA to ice VII in pressure-temperature stability field of ice VIII.[11] It will be shown that the smaller interfacial energy between the SW and ice VII underlies the formation of the metastable ice VII phase in stable ice VI region, signaling similar local order of dense water and ice VII.

EXPERIMENTS

Precise and tunable control of de/compression rates has been a formidable challenge to high-pressure physics experiments. This limitation has hindered studies of nucleation and transition dynamics along pressure-induced phase transformation pathways; thus, the formation of ice VII phase in the region of ice VI phase has been sparsely reported.[17] To address this situation, we have developed a novel device, called the dynamic diamond anvil cell (dDAC), which enables us to apply a controlled time-dependent load (or pressure) on a sample over a wide range of de/compression rates.

The fundamental design of dDAC adapts that of a traditional DAC, which integrates electromechanical piezoactuators (Piezosystem Jena, PAHL) to control the load on the sample. Three piezoactuators, driven by a function generator and concentrically mounted on the cell, vary the load on the two diamond anvils and thus modulate the load on the tip of diamond anvils (i.e., the pressure of the sample). Utilizing various driving wave forms (step, ramp, saw, sinusoidal, etc.), we can precisely control the amount of pressure change (0.1–10 GPa), frequency (0.1 mHz–20 kHz), and compression strain rate ($0.1-10^4$/sec) over an equally broad range of initial static high pressures (0.1–50 GPa). The piezodrive serves to change the sample thickness (and thus volume), which corresponds to a change in pressure depending on the sample's equation of state. In the case of a sample that remains in a single phase, the pressure will simply rise and fall monotonically proportional to the input voltage of piezoactuators, as shown in the time-pressure diagram of Fig. 2. However, in the case of a sample that undergoes a phase transformation, at the transformation pressure the sample pressure will stagnate and plateau, remaining constant while the relative volume fractions of the phases adjust as the sample transforms from one phase to the next, also shown in Fig. 2. Importantly, we find that the electronically driven pressure in the dDAC exhibits a minimum level of mechanical noise and perturbation, which is especially important for inhibiting phase transformations and achieving the supercompressed liquid state at high pressures.

We used high-pressure experimental instrumentation and techniques similar to those of previous high pressure studies.[18] We used 0.35-carat diamond anvils with 0.3 mm flat tips together with metal gaskets (0.25 mm initial thickness stainless steel or rhenium). High purity water (H_2O, Aldrich) was loaded into a small ~0.1 mm diameter, ~0.1 mm thick preindented gasket, together with a few submicron particles of ruby. The sample pressure was measured

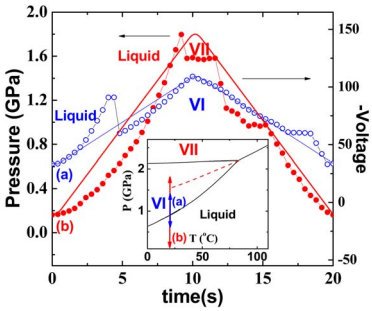

FIG. 2. (Color online) The pressure-time transformation paths of water at the de/compression rate of (a) 0.08 (blue-thin line) and (b) 0.16 (red-thick line) GPa/s. The inset depicts these processes in the pressure-temperature phase diagram of H_2O reproduced from Ref. 22. The symbols and lines are real-time measured pressures and applied voltages of the sample in the dDAC. The pressure uncertainty is estimated to be ±0.02 GPa. The real-time movie clips of these experiments are also presented on-line in Suppl. A and B (Ref. 19).

in real time using the ruby luminescence with a time resolution of 100 ms. In order to avoid heating by the excitation laser, we typically used only a few mW of 514.5 nm laser power for the ruby fluorescence and Raman. A thermocouple is attached to a diamond surface near the gasket hole to measure any temperature change. We found no measurable temperature change during the entire experiments due to friction and phase transformation, presumably because of large mass of diamond anvils with respect to a relatively small temperature variation of the sample. The phases of water and ice were identified based on the optical image (captured with a Sony video camera) and the Raman spectrum.

RESULTS

Figure 2 displays a time record of the drive voltage (solid lines) and pressure (symbols) of a H_2O sample in the dDAC at the compression rates of (a) 0.08 GPa/s (blue-thin line) and (b) 0.16 GPa/s (red-thick line). The corresponding pressure change is measured *in situ* by ruby luminescence as shown in Fig. 3. The inset depicts the thermodynamic pathways on the phase diagram of H_2O. Note that the drive voltage approximately corresponds to the displacement of the piezo and thus the sample volume. Therefore, the discontinuous jump in pressure is an indication of a phase change. Based on these pressure-time traces and the optical images presented in Supplement A and B,[19] we infer that water is compressed without crystallization to well beyond the equilibrium freezing pressure of 0.9 GPa prior to its transformation to denser ice VI or ice VII, depending on the rate of compression. At the slow compression rate [Fig. 2(a)], the sudden pressure drop from 1.2 GPa to 0.9 GPa is evidence of the solidification of water. The absence of a plateau after the sharp drop in pressure indicates that the supercompressed water was totally transformed to ice VI during the drop. On the other hand later in time, the pressure plateau at 0.9 GPa indicates a two-phase region of water and ice VI at the transition. The optical image at 0.9 GPa (Supplement *A*) is also consistent with that of a two-phase mixture.

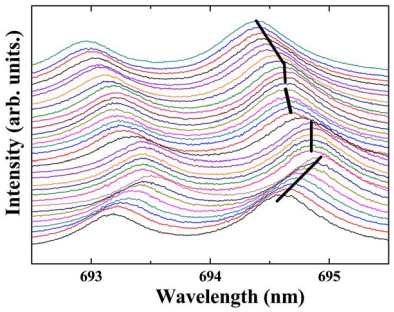

FIG. 3. (Color online) Time-resolved ruby luminescence, *in situ*, measured along the compression path of Fig. 2(b), from which the pressures are determined (open symbols in Fig 2(b). The solid line represents the $R1$ peak position, signifying the one-to-one correspondence between the Ruby peak shifts and the pressures jumps. The solid straight lines on $R1$ peak are for eye-guide.

At the higher compression rate [Fig. 2(b)], water is metastably supercompressed without crystallization to even higher pressures and undergoes two crystallization events which are signified by the sudden pressure drops at 1.8 and 1.58 GPa. Prior to the first pressure drop, the sample shows no distinct crystal grain boundaries or morphology, clearly indicating liquid water [Figs. 4(a) and 5(a)]. Note that the plateau at 1.58 GPa following the first pressure drop at 1.8 GPa is around the onset of the extrapolated melt line of ice VII at ambient temperature (Fig. 2 inset). The first pressure drop, thus, indicates the formation of a denser crystalline phase than the supercompressed water. The crystalline phase has a long platelike morphology [Fig. 4(b), and Supplement *B*] and its Raman spectrum[20] is clearly that of ice VII [Fig. 5(b)]. At the first pressure plateau, we found water at the crystal boundaries, and the crystals and water disappear abruptly (within 30 ms) at the end of the plateau and reappear at the second pressure drop to 1.1 GPa. Then, the crystalline phase further evolves to ice VI [Figs. 4(c) and 5(c)] that completely melts to water at the end of the plateau at around 0.96 GPa. A small drift in pressure immediately following the second pressure drop to 1.1 GPa may indicate the presence of yet another phase prior to the formation of ice VI, which could be ice XII phase, previously suggested to melt at around 1.0 GPa,[21] However, Raman spectra and optical images in this experiment do not provide definitive evidence for the presence of ice XII.

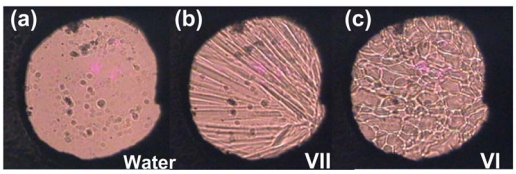

FIG. 4. (Color online) Optical images of the phases taken during the 0.16 GPa/s experiment in Fig. 2(b): (a) water, (b) ice VII, and (c) ice VI. These images are taken for 33 ms and selected from on-line Supp. B (Ref. 19). Spots in the cell are ruby particles and chips from the gasket. Since pristine samples showed the same crystallization sequences, it implies that the spots/impurities do not influence or effect the crystallization.

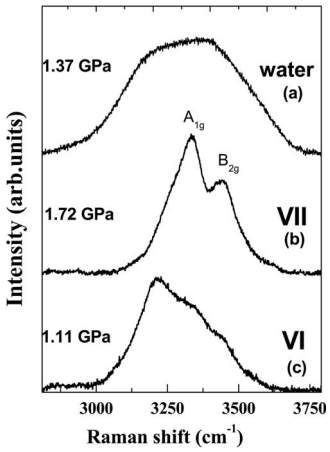

FIG. 5. Raman spectra of the phases arising from the 0.16 GPa/s experiments in Fig. 2(b): (a) water, (b) ice VII and (c) ice VI. The Raman spectra of ice VII and ice VI were obtained from the single phases synthesized at the indicated pressures, slightly elevated from the two-phase mixture regions of 1.58 GPa and 0.96 GPa in Fig. 2(b).

It is surprising that liquid water is compressed up to 1.8 GPa at 20 °C without crystallization, which corresponds to approximately 46 °C of undercooling at 1.8 GPa from ice VI melting.[22] Note that such a deep supercompression (~75% of ice VI stability region) of liquid water has never been observed in static high pressures study. Furthermore, neither has it been seen in any previous undercooling experiments to form metastable ice VII phase under similar high-pressure conditions (1.8 GPa). For comparison, the previous experiment of water at 0.7 GPa has shown an undercooling of 13 K prior to the formation of ice VI,[23] substantially smaller than 46 K what we observed in the present study. The undercooling value of the previous experiments, ΔT_r $[=(T_m-T_r)/T_m$ (where, T_m is melting temperature, and T_r is nucleation temperature] corresponds to 0.05-0.06, signaling heterogeneous nucleation. At ambient pressure, the homogeneous nucleation of liquid water happens about 40 K below melting temperature ($\Delta T_r=0.15$),[24,25] similar to the value 46 K observed in the present experiments. The undercooling 46 K at 1.8 GPa corresponds to an undercooling value of 0.14, for ice VI. Since stability limit conjecture temperature which is usually lower than homogeneous nucleation temperature is located 40 K below the melting at 1.8 GPa,[26] the undercooling in this study may be quite close to the homogeneous nucleation temperature although it should be higher than the temperature.

DISCUSSION

The most surprising observation of the present study is the formation of metastable ice VII from supercompressed water (SW) well within the stability regime of ice VI. This observation is also analogous to the previous result[11] that metastable ice VII-like phase forms from HDA at low temperature well within the stability regime of ice VIII phase. Combining these two results, one can raise important ques-

tions: why does metastable ice VII form from the disordered phases in the stable phase field of ice VI and ice VIII? Do reported[9,10,12–14] similarities in the local order of water and ice VII underlie this unexpected transformation? In fact, recent structural and thermodynamic studies have revealed that local order influences phase selection.[6–8] That is, the similarity of local order between liquids and solids leads to lower interfacial energy, and thus, a lower nucleation barrier and easier nucleation, even for metastable phases. Therefore, if the local structure of high density water is bcc-like, it is expected that the supercompressed water should show a smaller interfacial energy with ice VII phase than with ice VI phase. Ice VII can be metastably formed at 47 °C at 1.8 GPa, based on the extrapolated melting curve of ice VII, and thus a relatively small undercooling value, 27 K ($\Delta T_r = 0.084$) is obtained. This small undercooling reflects smaller nucleation barrier originated from smaller interfacial energy between supercompressed water (SW) and ice VII. To confirm this, we calculate the interfacial energies of SW/VII and SW/VI phases using classical nucleation theory. Here, homogeneous nucleation is assumed, since the deep undercooling 46 K obtained in present study may be close to homogeneous nucleation limit.

From the thermodynamic perspective, the phase selection can be understood in terms of two competing factors: the Gibbs free energy difference, Δg (driving force) and the interfacial free energy, σ (causing energy barrier) in classical nucleation theory. Formation of a new phase requires work, overcoming a nucleation barrier W^* composed of the two quantities[25]

$$W^* = 16\pi\sigma^3/[3(\Delta g)^2]. \quad (1)$$

Here, these thermodynamic quantities can be implicitly related to the local structures of the new and old phases. Therefore, we first estimate the difference of Gibbs free energy, Δg between the two phases governing the nucleation barrier. At given constant temperature, the difference in Gibbs free energy between the supercompressed liquid and crystalline phases can be written as

$$\Delta g = \Delta G^{ls}/m = \left(\int \Delta V^{ls} dP\right)/m = \Delta V^{ls}\Delta P/m$$
$$= [(\rho^s - \rho^l)/\rho^s\rho^l]^*\Delta P, \quad (2)$$

where m is the specific mass and the l and s indicate liquid and solid, respectively. The volume difference between liquid water and ice ($\Delta V^{ls} = V^l - V^s$) is approximated to be independent of pressure, and ΔP is the supercompressed pressure increment over the equilibrium melting pressure (plateaus in Fig. 2). Then, we estimate Δg to be 329 J/mol for ice VII and 432 J/mol for ice VI [ρ^s(VII)=1.532 (g/cm^3), ρ^s(VI) =1.394 (g/cm^3) and ρ^l (liquid water)=1.344 (g/cm^3) at 1.8 GPa, and $\Delta P = 0.2 (= 1.8 - 1.6)$ GPa for ice VII and 0.9 (=1.8–0.9) GPa for ice VI, and also see parameters to obtain density in Table I]. This is consistent with common expectation, i.e., smaller the driving energy for the metastable phase than for the stable phase.

Since the larger driving force Δg leads to a smaller nucleation barrier W^* as in Eq. (1), ice VII should not nucleate in the stability region of ice VI. This is clearly contrary to the present observation of metastable ice VII within the stable ice VI phase region and suggests that the other factor, the interfacial energy, is important for the phase selection. Here, we estimate the interfacial energy as the following (see Ref. 25). Consider an ensemble of droplets of uniform size, v, the probability of having no nuclei in a given N nuclei per mole is $X = \exp(-vn)$. Assuming steady state nucleation at the rate $I[P(t)]$ and that the liquid droplet is undercooled at the compression rate (or cooling rate) q from the melting pressure P_m (or temperature T_m), to maximum undercooling pressure P_r (or temperature T_r), the probability of no nucleation event is $X = \exp\{-v\int I[P(t)]dt\}$. Therefore, when the nucleation occurs, the production of sample volume, nucleation rate, and nucleation time, $\Sigma\, vI(P_i)\Delta t$, should be greater than one at the nucleation pressure (or temperature).[25] The time that the sample remains at each pressure or temperature can be calculated from the compression curve or cooling curve. Note that this calculation is only possible because the pressure-time curve (Fig. 2) can be measured in this dDAC experiment.

TABLE I. Used parameters for density extrapolation with a third-order Birch-Murnaghan equation (Ref. 31).

	ρ_o (g/cm^3)	K_{oT} (GPa)	K_{oT}
Water (Ref. 27)	0.99515	2.15	7.3
Ice VI (Ref. 28)	1.23729	10	7.1
Ice VII (Ref. 29)	1.4661	21	4.5

The steady state nucleation rate per unit volume at temperature T is given by[25]

$$I^s = \frac{6n^{*2/3}k_BTN_A}{\pi\lambda^3\eta}\left(\frac{\delta\mu}{6\pi k_BTn^*}\right)^{1/2}\exp\left(-\frac{W^*}{k_BT}\right), \quad (3)$$

where, $\eta(P)$, $\lambda(P)$, $n^*(P)$ [$=32\pi\sigma^3/3v(\Delta g/v)^3$, v is molar volume], and $\delta\mu(=\Delta g/N_A)$, and W^* are the viscosity, the average atomic jump distance, the number of atoms in the critical size of nucleus, the Gibbs free energy difference between the initial and final phases per atom (driving free energy), and the work of critical cluster formation, respectively; k_B is Boltzmann constant and N_A is the Avogadro's number. Note that for the present study, at constant temperature, the viscosity, Gibbs energy and nucleation barrier, and thus nucleation rate are functions of pressure.

Recall that nucleation is a fluctuation phenomenon that small clusters aggregate as the result of stochastic movement of atoms or molecules across interface. Therefore, the rate of nucleation should follow Boltzmann distribution at given temperature.[25] Under this circumstance, the applied pressure changes two aspects of nucleation; the stability of the clusters governed by Gibbs free energy difference between two phases and the atomic (or molecular) jump rate across interface which is related to viscosity. The stability can be determined by pressure in Eqs. (1) and (2). Pressure dependence of viscosity is same as temperature dependence.[30] Therefore,

TABLE II. Calculated interfacial energies with different fitting functions for viscosity. VFTH and polynomial function give better fitting than Arrhenius function.

	Fitting functions for viscosity (poise) (Ref. 32)		
	Arrhenius (Ref. 30)	VFTH (Ref. 30)	Polynomial
	$0.00859\exp[P\times 3.2654\times 10^{-30}/(1.38\times 10^{-23}\times 293)]$	$0.00912\exp[2.05455\times P/(3.67922\text{-}P)]$	$0.00945+0.00203P+0.00814P^2$
Interfacial energy (mJ/m^2)	29.34 (±0.01) (SW/VI) 23.02 (±0.01) (SW/VII)	29.23 (±0.01) (SW/VI) 22.93 (±0.01) (SW/VII)	29.33 (±0.01) (SW/VI) 23.01 (±0.01) (SW/VII)

the usage of Eq. (3) is still valid for the pressure-driven nucleation phenomena in the present study. Here, λ and the driving Gibbs free energy in Eq. (2) are estimated using the density data of water extrapolated up to 1.8 GPa at 20 °C, and the viscosity comes from the extrapolation of the previously reported data up to 1 GPa.[31] Thus the interfacial energy can be evaluated, which satisfies the inequality, $I^s(P_r)\cdot V\cdot t_r \geqslant 1$, with the given parameters. Although the absolute value by this method would not be guarantied due to the assumptions, this method has been successfully applied to show a good agreement with theoretical expectation.[6,8] Moreover, at least, the relative value obtained by the present method should be valid and reflect the difference of interfacial energy between the two phases. Calculated interfacial energies are summarized in Table II with different fitting functions for viscosity. Calculated interfacial energy between ice VI and liquid water is 29 (±0.9)mJ/m^2 by considering pressure uncertainty. This value is quite closed to 32 mJ/m^2, previously determined from an undercooling experiment at ambient pressure,[19] and theoretical values which were predicted from ambient pressure to 0.3 GPa by assuming homogeneous nucleation.[33] Smaller interfacial energy, 23 (±1.9)mJ/m^2 for ice VII is obtained as expected.

The present study clearly shows that the similarity of local orders between liquid and solid can lower interfacial energy between the two, which has long been predicted.[34] Recently, there are also numerous experimental evidences[7,8] unambiguously demonstrating the relationship between interfacial energy and local order. For example, supercooled TiZrNi alloy liquid crystallizes into metastable icosahedral crystalline phase (*i* phase) rather than stable C14 Laves phase (hcp), although the undercooling value (~0.09) of *I* phase is smaller than that of C14 Laves phase (~0.14). As described above, the calculated interfacial energy between the liquid and *i* phase is smaller than that between the liquid and C14 Laves phase (hcp). Furthermore, *in situ* x-ray diffraction study revealed that the local order of the alloy melt contains same icosahedral short range order in x-ray diffraction study as that of *i* phase. Clearly, the present result is very similar to the crystallization event occurring in TiZrNi alloy liquid. Therefore, the smaller interfacial energy of ice VII implies a similar local structure between the supercompressed dense water and ice VII rather than ice VI.

The supercompressed water at 1.8 GPa has features consistent with HDW, if one considers that the broad definition of HDW depends on coordination number. That is, HDW is thought to have similar coordination number to crystal structure, i.e., 8 to 12. For example, Wu[35] reported that the coordination number of water as HDW is 7.4 at 1.56 GPa and 85 °C in neutron scattering experiment. One can easily expect that the coordination number in present study might be higher than this, because of the higher pressure (1.8 GPa) and lower temperature (20 °C). In addition, the pressure range used in this study clearly passed over the boundary of LDW and HDW predicted by simulation study.[13] Therefore it is plausible to argue that high density water is achieved under the deep compression in this study, and the smaller interfacial energy for ice VII may support the recent simulation studies, showing that the local order of HDW is bcc-like, as in ice VII.[12–14]

SUMMARY

In summary, using a newly developed dDAC, we demonstrated that liquid water can be supercompressed into the thermodynamically stable pressure range of ice VI, 1.8 GPa at 20 °C. The pressure-time curves, measured for the first time, showed the interesting phase transformation sequences of supercompressed water–initially to metastable ice VII and water during compression, then to ice VI, and finally to liquid water during decompression. The smaller value of the interfacial energy of SW/ice VII in comparison to that of SW/ice VI, that we evaluated here, is a manifestation of the similarity of their local ordering. This is consistent with the local ordering similarity of HDW and ice VII, i.e., bcc-like order, and similarly HDA and ice VII.

ACKNOWLEDGMENTS

We thank Magnus Lipp, Brian Maddox, Bruce Baer, and Kenneth Visbeck for their experimental assistance. This work was performed in support of the Physical Data Research Program under the auspices of the U.S. DOE by the University of California, Lawrence Livermore National Laboratory under Contract No. W-7405-Eng-48.

[1] C. Cavazzoni, G. L. Chiarotti, S. Scandolo, E. Tosatti, M. Bernasconi, and M. Parrinello, Science **283**, 44 (1999).
[2] O. Mishima, L. D. Calvert, and E. Whalley, Nature (London) **310**, 393 (1984).
[3] S. Klotz, T. Strassle, G. Hamel, R. J. Nelmes, J. S. Loveday, G. Rousse, B. Canny, J. C. Chervin, and A. M. Saitta, Phys. Rev. Lett. **94**, 025506 (2005).
[4] T. Kawamoto, S. Ochiai, and H. Kagi, J. Chem. Phys. **120**, 5867 (2004).
[5] A. K. Soper and M. A. Ricci, Phys. Rev. Lett. **84**, 2881 (2000).
[6] D. Holland-Moritz, Int. J. Non-Equilib. Process. **11**, 169 (1998).
[7] K. F. Kelton, G. W. Lee, A. K. Gangopadhyay, R. W. Hyers, T. J. Rathz, J. R. Rogers, M. B. Robinson, and D. S. Robinson, Phys. Rev. Lett. **90**, 195504 (2003).
[8] G. W. Lee, A. K. Gangopadhyay, T. K. Croat, T. J. Rathz, R. W. Hyers, J. R. Rogers, and K. F. Kelton, Phys. Rev. B **72**, 174107 (2005).
[9] J. L. Finney, A. Hallbrucker, I. Kohl, A. K. Soper, and D. T. Bowron, Phys. Rev. Lett. **88**, 225503 (2002).
[10] S. Klotz, G. Hamel, J. S. Loveday, R. J. Nelmes, M. Guthrie, and A. K. Soper, Phys. Rev. Lett. **89**, 285502 (2002).
[11] R. J. Hemley, L. C. Chen, and H. K. Mao, Nature (London) **338**, 638 (1989).
[12] M. Canpolat, F. W. Starr, A. Scala, M. R. Sadr-Lahijany, O. Mishima, S. Havlin, and H. E. Stanley, Chem. Phys. Lett. **294**, 9 (1998).
[13] A. M. Saitta and F. Datchi, Phys. Rev. E **67**, 020201(R) (2003).
[14] E. Schwegler, G. Galli, and F. Gygi, Phys. Rev. Lett. **84**, 2429 (2000).
[15] D. H. Dolan and Y. M. Gupta, Chem. Phys. Lett. **374**, 608 (2003); J. Chem. Phys. **121**, 9050 (2004).
[16] J. A. Moriarty, J. F. Belak, R. E. Rudd, P. Söderlind, F. H. Streitz, and F. H. Yang, J. Phys.: Condens. Matter **14**, 2825 (2002).
[17] S. N. Tkachev, R. M. Nasimov, and V. A. Kalinin, J. Chem. Phys. **105**, 3722 (1996); K. Yamamoto, Jpn. J. Appl. Phys. **19**, 1841 (1980).
[18] W. J. Evans, M. J. Lipp, H. Cynn, C. S. Yoo, M. Somayazulu, D. Hausermann, G. Shen, and V. Prakapenka, Phys. Rev. B **72**, 094113 (2005).
[19] See EPAPS Document No. E-PRBMDO-74–034637 for movie clips of the experiments. Supp. A is a movie clip recorded during the 0.08 GPa/s experiment in Fig. 2(a), showing supercompressed water-ice VI—water transformations. Supp. B is a movie clip taken during the 0.16 GPa/s experiment in Fig. 2(b), showing supercompressed water—metastable ice VII—ice VI—water transformations. This document can be reached via a direct link in the online article's HTML reference section or via the EPAPS homepage (http://www.aip.org/pubservs/epaps.html).
[20] G. E. Walrafen, M. Abebe, F. A. Mauer, S. Block, G. J. Piermarini, and R. Munro, J. Chem. Phys. **77**, 2166 (1982).
[21] I. M. Chou, J. G. Blank, A. F. Goncharov, H. K. Mao, and R. J. Hemley, Science **281**, 809 (1998).
[22] W. Wagner, A. Saul, and A. Pruß, J. Phys. Chem. Ref. Data **23**, 515 (1994).
[23] A. D. Molina-Garcia, L. Otero, M. N. Martino, N. E. Zaritzky, J. Arabas, J. Szczepek, and P. D. Sanz, Meat Sci. **66**, 709 (2004).
[24] R. J. Speedy, J. Phys. Chem. **86**, 982 (1982).
[25] K. F. Kelton, Solid State Phys. **45**, 75 (1991).
[26] A. K. Soper, Science **297**, 1288 (2002).
[27] A. Span and W. Wagner, J. Phys. Chem. Ref. Data **18**, 1538 (1989).
[28] A. Polian and M. Grimsditch, Phys. Rev. B **27**, 6409 (1983).
[29] M. R. Frank, Y. Fei, and J. Hu, Geochim. Cosmochim. Acta **68**, 2781 (2004).
[30] C. M. Roland, S. Hensel-Bielowka, M. Paluch, and R. Casalini, Rep. Prog. Phys. **68**, 1405 (2005).
[31] F. Birch, J. Geophys. Res. **83**, 1257 (1978).
[32] K. E. Bett and J. B. Cappi, Nature (London) **207**, 620 (1965), H. E. King, Jr. E. Herbolzheimer, and R. L. Cook, J. Appl. Phys. **71**, 2071 (1992).
[33] S. N. Luo, A. Strachan, and D. C. Swift, Modell. Simul. Mater. Sci. Eng. **13**, 321 (2005).
[34] F. C. Frank, Proc. R. Soc. London **215**, 43 (1952).
[35] A. Y. Wu, E. Whalley, and G. Dolling, Chem. Phys. Lett. **84**, 433 (1981).